Membrane contact site detection (MCS-DETECT) reveals dual control of rough mitochondria–ER contacts

Ben Cardoen[1]*, Kurt Vandevoorde[2]*, Guang Gao[2]*, **Milene Ortiz-Silva**[2]*, Parsa Alan[2], William Liu[2], Ellie Tiliakou[2], A. Wayne Vogl[2], Ghassan Hamarneh[1]#, Ivan R. Nabi[2,3]#

*, # equal contribution # To whom correspondence should be sent: hamarneh@sfu.ca; irnabi@mail.ubc.ca

[1]School of Computing Science, Simon Fraser University, Burnaby, BC, Canada V5A 1S6 [2] Department of Cellular & Physiological Sciences, LSI, University of British Columbia, Vancouver, BC, Canada V6T 1Z3 [3]School of Biomedical Engineering, UBC, Vancouver, BC, Canada V6T 1Z3

Abstract

Identification and morphological analysis of mitochondria–ER contacts (MERCs) by fluorescent microscopy is limited by subpixel resolution interorganelle distances. Here, the membrane contact site (MCS) detection algorithm, MCS-DETECT, reconstructs subpixel resolution MERCs from 3D super-resolution image volumes. MCS-DETECT shows that elongated ribosome-studded riboMERCs, present in HT-1080 but not COS-7 cells, are morphologically distinct from smaller smooth contacts and larger contacts induced by mitochondria–ER linker expression in COS-7 cells. RiboMERC formation is associated with increased mitochondrial potential, reduced in Gp78 knockout HT-1080 cells and induced by Gp78 ubiquitin ligase activity in COS-7 and HeLa cells. Knockdown of riboMERC tether RRBP1 eliminates riboMERCs in both wild-type and Gp78 knockout HT-1080 cells. By MCS-DETECT, Gp78-dependent riboMERCs present complex tubular shapes that intercalate between and contact multiple mitochondria. MCS-DETECT of 3D whole-cell super-resolution image volumes, therefore, identifies novel dual control of tubular riboMERCs, whose formation is dependent on RRBP1 and size modulated by Gp78 E3 ubiquitin ligase activity.

Distinct MERCs in COS-7 and HT-1080 cells

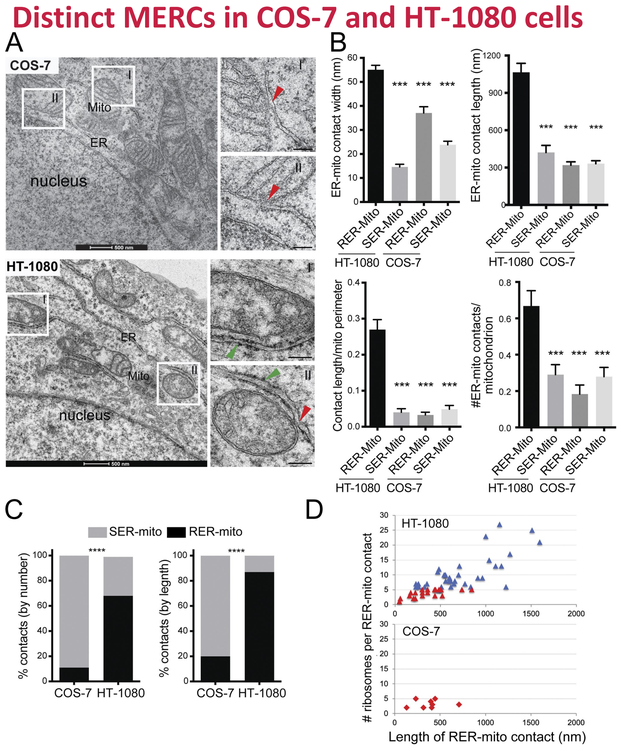

Figure 1. Quantitative EM analysis of ER–mitochondria contacts in HT-1080 and COS-7 cells. (A) Representative EM images of HT-1080 and COS-7 cells. Insets show rough ER–mitochondria contacts (RER-mito) in HT-1080 cells (green arrowheads) and smooth ER–mitochondria contacts (SER-mito) in HT-1080 and COS-7 cells (red arrowheads). **(B)** Quantification of contact width, contact length, contact length relative to mitochondria perimeter, and number of contacts per mitochondria profile are shown for SER-mito and RER-mito contacts in HT1080 and COS-7 cells. **(C)** The relative ratio of SER-mito and RER-mito contacts in HT-1080 and COS-7 cells based on the number of contacts per mitochondria or length of contacts. **(D)** The number of ribosomes per RER-mito contact is plotted versus the length of the contact in nm for HT-1080 and COS-7 cells. RER-mito contacts with five or less ribosomes are shown in red; those with more than five ribosomes are specific to HT-1080 cells and are shown in blue and defined as riboMERCs. *n* = 27 images from two independent biological replicates; ±SEM; ***P < 0.001; ****P < 0.0001; B: one-way ANOVA; C: Chi2 test. Bar = 500 nm; inset: 200 nm.

MERC identification by differential channel correlation

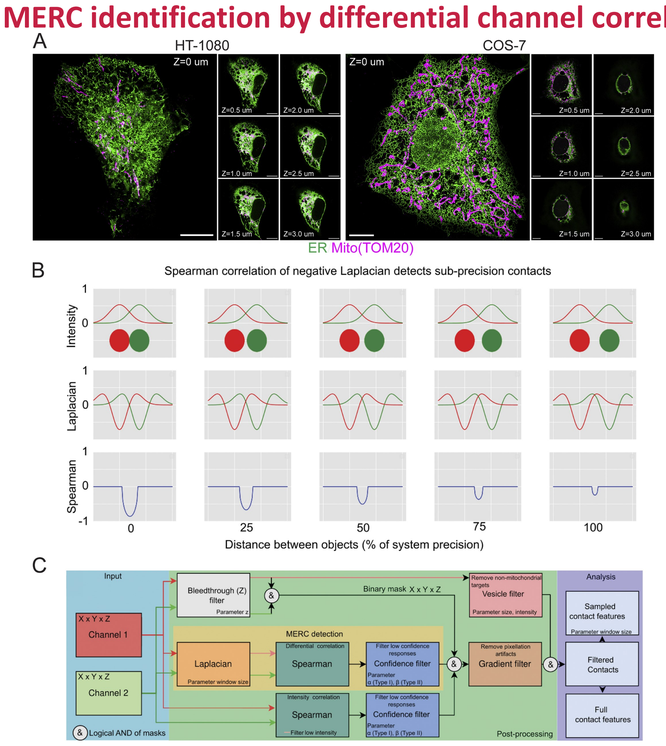

Figure 2. MCS-DETECT analysis of sub-precision contacts. (A) 3D STED images of HT-1080 and COS-7 showing overlap between mitochondria (magenta) and ER (green). Insets show STED sections at 0.5 µm Z spacing. Bars = 10 µm. **(B)** Two objects (red and green discs) are shown at corresponding sub-precision distances. Intensity profiles (top row), second derivatives (Laplacian), and Spearman correlations of the negative part of the Laplacian (bottom row) are shown. Note how the Spearman response overlaps and changes consistently with the sub-precision distance. **(C)** The detection algorithm (orange) with additional stages that each address a specific confounding factor introduced by the acquisition (bleed through) or sample (vesicle removal).

Detecting riboMERCs in HT-1080 cells with MCS-DETECT

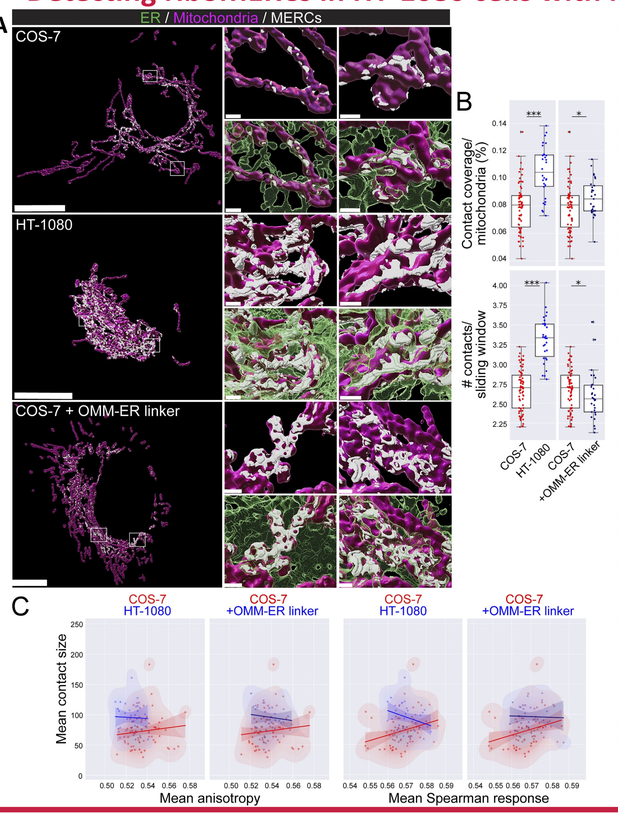

Figure 3. Subprecision contact detection identifies distinct contact profiles in HT-1080 and COS-7 cells. (A) Volume-rendered MCS-DETECT views of cells expressing ERmoxGFP (green) and labeled for TOM20 (magenta) with contact sites overlaid (white) are shown for COS-7, HT-1080, and OMM–ER linker transfected COS-7 cell ROIs from the whole view image are shown volume rendered in adjacent panels. COS-7 mitochondria display numerous small contact zones while mitochondria in HT-1080 and OMM–ER linker transfected COS-7 cells present more extended contact zones (bar = 10 µm whole cell; 1 µm insets). (B) Mitochondria surface coverage ratio and the number of contacts per sampled mitochondria window are shown for contact zones in COS-7, HT-1080, and OMM–ER linker transfected COS-7 cells (averaged over cell, two-sided non-parametric Mann Whitney test, n = 3 independent biological replicates, ≥30 cells/condition per experiment; *P < 0.05; ***P < 0.001). (C) 2D KDE plots of mean contact size over mean anisotropy and mean Spearman response, with a linear regression overlayed, are shown for COS-7 (red) versus HT-1080 (blue) cells or COS-7 (red) versus OMM–ER linker transfected COS-7 (blue) cells..

Gp78 regulation of riboMERC expression and mitochondrial potential

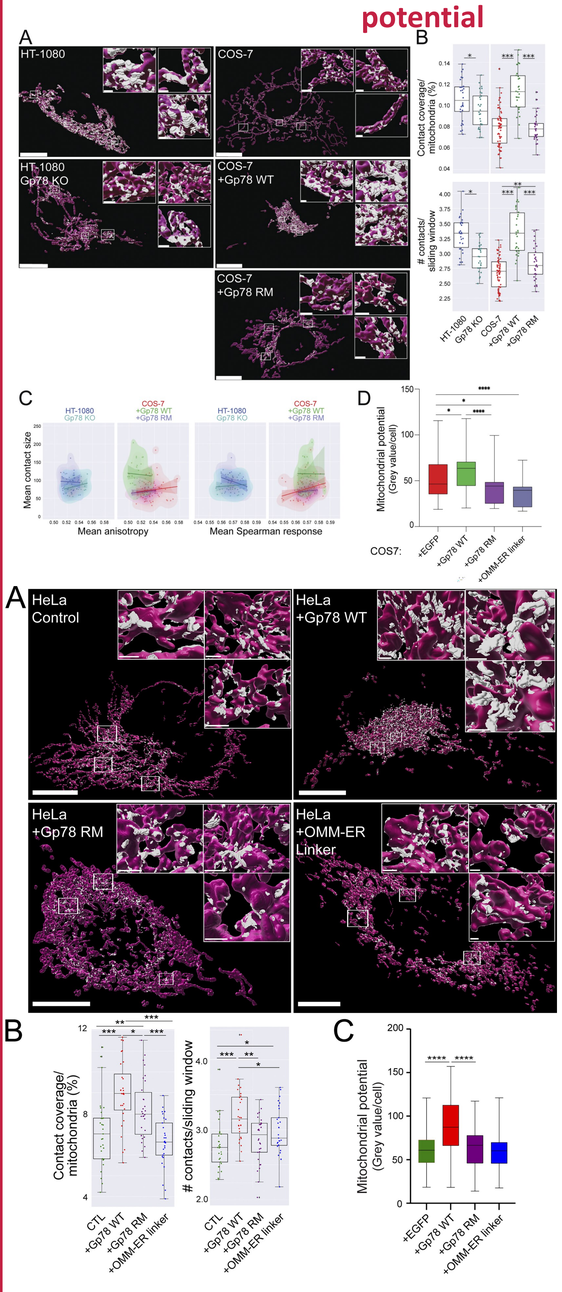

Figure 4. Gp78 regulation of riboMERCs. (A) Volume-rendered MCS-DETECT views of cells expressing ERmoxGFP and labeled for TOM20 (magenta) with contact sites overlaid (white) are shown for HT-1080 and Gp78 KO HT-1080 cells and for untransfected COS-7 cells and COS-7 cells overexpressing WT Gp78 or Gp78 RM. Bar = 10 µm whole cell; 1 µm insets. (B) Mitochondria surface coverage ratio and the number of contacts per sampled mitochondria window are shown for contact zones in HT-1080 and Gp78 KO HT-1080 cells and for untransfected COS-7 cells and COS-7 cells overexpressing Gp78 WT or Gp78 RM. (C) 2D KDE plots of mean contact size over mean anisotropy and mean Spearman response, with a linear regression overlayed, are shown for HT-1080 (blue) versus Gp78 KO HT-1080 (green) cells or COS-7 (red) versus COS-7 overexpressing either Gp78 WT (green) or Gp78 RM (blue). Averaged over cell, n = 3 independent biological replicates, ≥30 cells/condition per experiment; *P < 0.05; **P < 0.01; ***P < 0.001, two-sided non-parametric Mann–Whitney test. (D) COS-7 cells were transfected with EGFP (as a control), Gp78 WT IRES-GFP, Gp78 RM IRES-GFP, or the OMM–ER linker (RFP) and labeled with MitoView 633. Integrated density of MitoView 633 per cell was quantified. n = 3 independent biological replicates; >35 cells/condition per experiment; *P < 0.05; ****P < 0.0001; Tukey post hoc test.

Figure 5 Gp78 induces riboMERCs in HeLa cells. (A) Volume-rendered MCS-DETECT views of cells expressing ERmoxGFP and labeled for TOM20 (magenta) with contact sites overlaid (white) are shown for untransfected HeLa cells and HeLa cells overexpressing WT Gp78, Gp78 RM, and the OMM–ER linker. Bar = 10 µm whole cell; 1 µm insets). (B) Mitochondria surface coverage ratio and the number of contacts per sampled mitochondria window are shown for contact zones in the cells indicated above. Averaged over cell, two-sided non-parametric Mann–Whitney test, n = 3 independent biological replicates, ≥30 cells/condition per experiment; *P < 0.05; **P < 0.01; ***P < 0.001. (C) HeLa cells were transfected with EGFP (as a control), Gp78 WT, Gp78 RM, or the OMM–ER linker and labeled with MitoView 633. Integrated density of MitoView 633 per cell was quantified. n = 3 independent biological replicates; >35 cells/condition per experiment; ****P < 0.0001; Tukey post hoc test.

Gp78 and RRBP1 are independent regulators of riboMERC expression

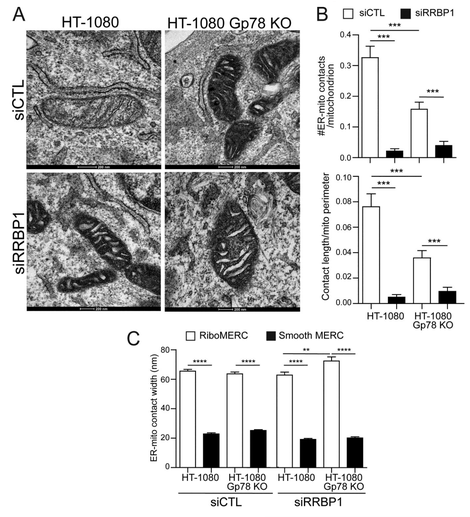

Figure 6. RRBP1 knockdown reduces riboMERCS independent of Gp78. (A) Representative EM images of HT-1080 and HT-1080 Gp78 KO cells treated with either siControl or siRRBP1. Images highlight the presence of riboMERCS in both HT-1080 WT and Gp78 KO cells, which are almost completely lost upon RRBP1 knockdown. (B) Quantification of the number of riboMERCs per mitochondria and the ratio of riboMERC length to mitochondrial perimeter for the conditions in A. (C) Quantification of the MERC width for both riboMERCs and smooth MERCs for the conditions in A. n = 31 images from two independent biological replicates; **P < 0.01; ***P < 0.001; ****P < 0.0001; unpaired t test. Bar = 200 nm.

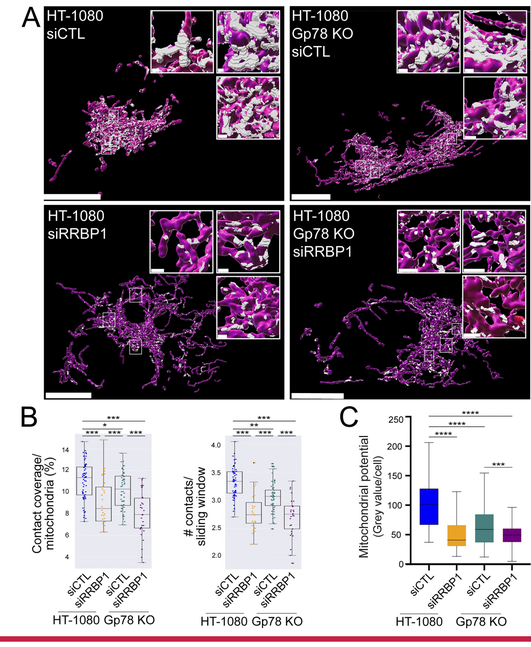

Figure 7. MCS-DETECT captures MERC changes induced by RRBP1 knockdown. (A) Volume-rendered MCS-DETECT views of HT-1080 WT and Gp78 KO cells treated with either siControl or siRRBP1. Mitochondria are labeled with TOMM20 (red) and MERCS are visualized in white. Bar = 10 µm whole cell; 1 µm insets. (B) Mitochondria surface coverage ratio and the number of contacts per sampled mitochondria window are shown for contact zones in HT-1080 WT and Gp78 KO cells treated with either siControl or siRRBP1. Averaged over cell, two-sided non-parametric Mann–Whitney test, n = 3 independent biological replicates, ≥30 cells/condition per experiment; *P < 0.05; **P < 0.01; ***P < 0.001. (C) HT-1080 cells transfected with either siControl or siRRBP1 were labeled with MitoView633. Integrated density of MitoView633 per cell was quantified. n = 3 independent biological replicates; >50 cells/condition per experiment; ***P < 0.0001; ****P < 0.0001; Tukey post hoc test.

Gp78-dependent riboMERCs present a distinct tubular morphology

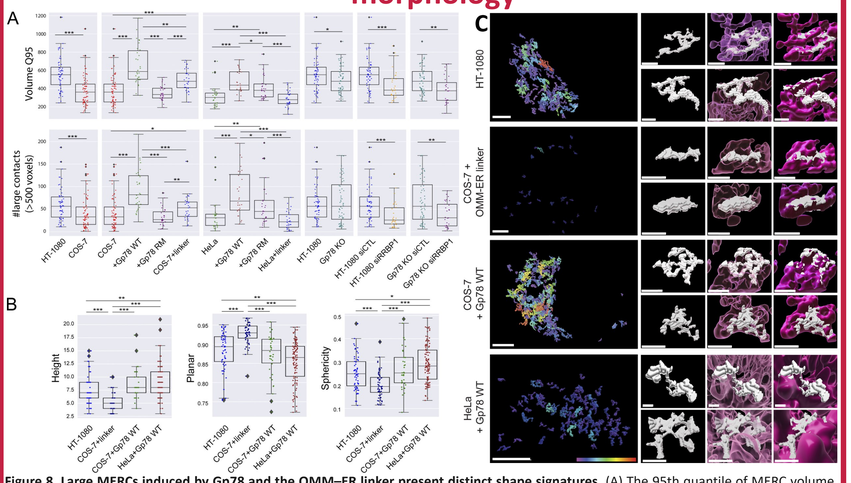

Figure 8. Large MERCs induced by Gp78 and the OMM–ER linker present distinct shape signatures. (A) The 95th quantile of MERC volume per cell (Q95V; largest 5% of MERCs per cell) and number of MERCs per cell larger than the average 500-voxel size of HT-1080 Q95V MERCs are shown for HT-1080 and COS-7 cells, COS-7, and COS-7 cells overexpressing either Gp78 WT, Gp78 RM, or the OMM–ER linker, HeLa and HeLa cells overexpressing either Gp78 WT, Gp78 RM, or the OMM–ER linker, HT-1080, and Gp78 KO HT-1080 cells, HT-1080 cells transfected with siCTL and siRRBP1, and Gp78 KO HT-1080 cells transfected with siCTL and siRRBP1. (B) Representative cells whose Q95V is closest to the mean Q95V for HT-1080 cells, for COS-7 or HeLa cells overexpressing Gp78 WT, and for COS-7 cells overexpressing the OMM–ER linker were selected for analysis. For the Q95V contacts of each cell, we compute shape features: height, sphericity, and planarity. The comparison shows that the COS-7 OMM–ER linker–induced contacts have a markedly different shape signature compared to those present in HT-1080 and Gp78 overexpressing COS-7 or HeLa cells (i.e., riboMERCS). (C) Representative whole-cell views of Q95V MERCs (color-coded for increasing size from 500 to 5,613 voxels) from HT-1080 cells, COS-7, or HeLa cells overexpressing Gp78 WT and COS-7 cells overexpressing the OMM–ER linker as well as representative individual Q95V MERCs alone or adjacent to transparent (pink) or solid mitochondria (magenta) to highlight intercalation of riboMERCs with mitochondria. Bar = 1 µm. Averaged over cell, two-sided non-parametric Mann–Whitney test, n = 3 independent biological replicates, ≥30 cells/condition per experiment; *P < 0.05; **P < 0.01; ***P < 0.001.

NSERC CRSNG
INNOVATION
Canada Foundation for Innovation
Fondation canadienne pour l'innovation
CIHR IRSC
Canadian Institutes of Health Research
Instituts de recherche en santé du Canada

Cardoen et al, 2024
doi.org/10.1083/jcb.202206109